Thermodynamic Properties of Magnesium-Boron Binary Alloys Determined Using Solid-State Electrochemical Measurements

MUHAMMAD A. IMAM and RAMANA G. REDDY

This study provides the thermodynamic properties of the Mg-B binary alloys. Experiments were performed to measure the electromotive force (emf) as a function of temperature (773 K to 873 K) using a solid-state electrochemical cells that can be represented as

$$(-)\mathrm{Pt, Ar}/\{\mathrm{Mg} + \mathrm{CaF_2} \cdot \mathrm{MgF_2}\}\|\mathrm{CaF_2}\|\{\mathrm{Mg(alloy)} + \mathrm{CaF_2} \cdot \mathrm{MgF_2}\}/\mathrm{Ar, Pt}(+)$$

The activities of Mg in Mg-B alloys were calculated from the experimental emf data. The activity coefficients of Mg in Mg-B alloys were also determined. The integral Gibbs energies of formation (ΔG_f°) of alloys were calculated from the activities of the Mg using tangent rule. The integral Gibbs energies of formation (ΔG_f°) of MgB_2, MgB_4, and MgB_7 are − 15.48, − 22.03, and − 15.89 kJ/mol-atoms at 873 K.

https://doi.org/10.1007/s11663-018-1392-7

I. INTRODUCTION

AFTER the discovery of the MgB_2 superconducting phase at 39 K,[1] the Mg-B binary system drew attention for further studies. The Mg-B binary system contains intermediate compounds, such as MgB_2, MgB_4, and MgB_7. In this binary system, it has semiconducting phases, like MgB_4 and MgB_7, which could be good candidates for high-temperature thermoelectric applications. MgB_4 has already been reported as a high-temperature thermoelectric material.[2] The other intermediate phases Mg_3B_2,[3] MgB_6, and MgB_{12}[4] are also reported in the early literature. However, they have not been confirmed yet with the further experimental evidence. Low-purity materials in the initial experiments, or the mixture of unstable borides and/or boron, were accountable for these phases.[5] In addition, based on Spear's[6] assessment, Massalski reported the Mg-B phase diagram,[7] which also confirmed the three intermediate phases MgB_2, MgB_4, and MgB_7. Recently, Liu *et al.*[8] and Kim *et al.*[9] used CALPHAD and *ab initio* calculations to reassess the Mg-B binary phase diagram. Their study did not confirm the Mg_3B_2, MgB_6, and MgB_{12} phases. The phases present in Mg-B system and their crystallographic structures are summarized in Table I. These theoretical studies reproduced the phases reported by Massalski.[7] Thermo-Calc and PANDAT also corroborated the same in the literature.[10,11] Although all three boride phases are reported as stoichiometric compound,[12] several studies found the small homogeneity of the boride phases.[2,13–18] The phase diagram of Mg-B system obtained from Thermo-Calc is shown in Figure 1.[10] The literature has also reported the different decomposition temperatures of these phases, which are summarized in Table II. This might be due to the limited availability of experimental data and different sources of thermodynamic database employed in a CALPHAD method.

Experimental difficulties arise for Mg due to its chemical reactivity and high vapor pressure at high temperature.[19] Thus, the thermodynamic data for Mg-B binary system have been limited to a few experimental phase equilibria studies. Cook *et al.* carried out vapor pressure and enthalpy measurements using Knudsen effusion vacuum thermogravimetry and calorimetry over the temperature range of 873 K to 1123 K.[20] In their study, they limited their measurements up to 0.8 mole fraction of boron. Thus, the thermodynamic properties of Mg-B alloy beyond 0.8 mole fraction were not reported. In another study, Brutti *et al.* performed vapor pressure measurements using a Knudsen spectrometry technique over the range of 883 K to 1154 K.[21]

MUHAMMAD A. IMAM and RAMANA G. REDDY are with the Department of Metallurgical and Materials Engineering, The University of Alabama, Tuscaloosa, AL 35487. Contact e-mail: rreddy@eng.ua.edu

Manuscript submitted June 12, 2017.
Article published online August 21, 2018.

Table I. Different Phases and Their Crystallographic Structures in the Mg-B System[30]

Phase	Approximate Composition (X_B)	Pearson Symbol	Prototype/Crystal Structure	Hermann Mauguin
(Mg)	0 to 0.66	*hP*2	Mg/HCP	$P6_3/mmc$
MgB_2	0.67	*h*P3	AlB_2	$P6/mmm$
MgB_4	0.8	*o*P20	MgB_4	*Pnma*
MgB_7	0.87	*o*I64	MgB_7	*Imma*
(B)	> 0.88	*h*R12	ZrCl	$R\bar{3}m$

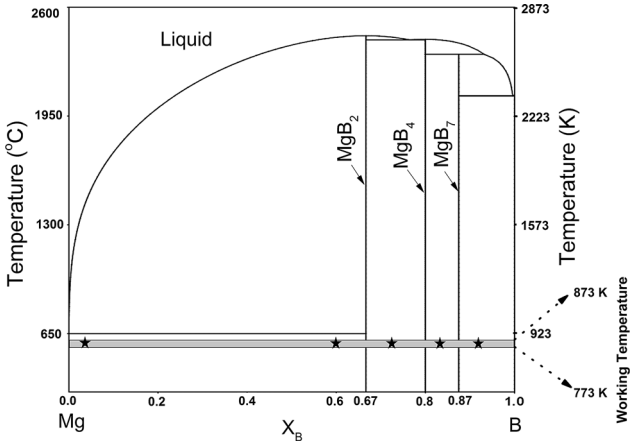

Fig. 1—Binary Mg-B phase diagram.[10]

To manage the high vapor pressure of Mg at a high-temperature range of 873 K to 1123 K reported,[20,21] we executed our thermodynamic measurements in the range of 773 K to 873 K in a pure solid-state electrochemical cell using a solid electrolyte. The Mg-B system was studied in the current study using solid-state electrochemical cell:

$$(-)\mathrm{Pt, Ar/\{Mg + CaF_2 \cdot MgF_2 \| CaF_2 \| \{Mg(alloy) + CaF_2 \cdot MgF_2\}/Ar, Pt(+).} \quad [1]$$

In this cell, solid Mg served as a reference electrode (RE), solid-state CaF_2 as an electrolyte, and solid Mg-B alloys as a working electrode (WE). Due to its superior chemical stability and higher ionic conductivity, CaF_2 was used in this study.[22,23] Solid-state CaF_2 electrolyte was widely utilized in the recent emf studies in the temperature range of 723 K to 1100 K.[24–28] It needs to be mentioned that a eutectic mixture of CaF_2 and MgF_2 ($X_{MgF_2} = 0.504$) was chosen to prepare the electrodes to preserve ionic conductivity.[29] Only metal fluoride, *i.e.*, MgF_2 could be used for this purpose, keeping in mind that metal fluoride tends to react with solid electrolyte CaF_2. The eutectic CaF_2-MgF_2 mixture was chosen for maintaining ionic conductivity in the electrodes to avoid any interaction with the cell electrolyte (CaF_2). It needs to be mentioned that the melting temperature of the CaF_2-MgF_2 eutectic mixture is 980 °C[30] which is above the experimental temperature range (500 °C to 600 °C).

Since fluoride-ion-conducting electrolyte CaF_2 is used, the half-cell reactions for the galvanic cell are

RE :

$$\mathrm{Mg(Solid) + CaF_2 + 2F^- = (CaF_2 \cdot MgF_2)(Solid) + 2e^-} \quad [2]$$

WEs :

$$\mathrm{(CaF_2 \cdot MgF_2)(Solid) + 2e^- = Mg(alloy) + CaF_2(Solid) + 2F^-.} \quad [3]$$

Equations [2] and [3] give the net cell reaction:

$$\mathrm{Mg(Solid) = Mg(alloy)(Solid).} \quad [4]$$

The change in the partial molar Gibbs energy of magnesium ($\Delta\bar{G}_{Mg}$) for the proceeding galvanic cell reaction is written as

$$\Delta\bar{G}_{Mg} = \Delta\bar{G}_{Mg(alloy)} - \Delta G^{\circ}_{Mg} \quad [5]$$

$$\Delta\bar{G}_{Mg} = RT\ln(a_{Mg(alloy)}/a_{Mg(S)}), \quad [6]$$

where $a_{Mg(alloy)}$ is the activity of Mg in Mg-B alloy, $a_{Mg(S)}$ is the activity of the pure magnesium, ΔG°_{Mg} is the standard partial molar Gibbs energy, R is the universal gas constant, and T is the absolute cell temperature. The measured equilibrium open-circuit potential, E_{cell}, is used in the Nernst equation (Eq. [7]) to obtain the partial molar Gibbs energy of Mg and the activity of Mg in Mg-B alloys.

$$\Delta\bar{G}_{Mg} = -nFE_{cell} \quad [7]$$

$$\ln a_{Mg(alloy)} = -\frac{nFE_{cell}}{RT}(a_{Mg(S)} = 1), \quad [8]$$

where n ($n = 2$) is the number of electrons participating in the half-cell reactions, and F is the Faraday constant ($F = 96{,}500$ C/mol). In the current study, the magnesium crystal (cr, $P6_3/mmc$) at each cell temperature T (773 K to 873 K) and the ambient pressure was selected as the standard state.

The more reliable and accurate thermodynamic data were measured after obtaining an equilibrium state in a solid-state galvanic cell. These equilibrium thermodynamic data can be used in the optimization of the phase boundary calculations for the Mg-B system.

Table II. Comparison of Phase Decomposition Temperatures from Different Literature Sources for Mg-B System

Phase	Massalski *et al.*[7] (Calc.) (°C)	Liu *et al.*[8] (Calc.) (°C)	Kim *et al.*[9] (Calc.) (°C)	Cook *et al.*[20] (Exp.) (°C)
MgB_2	1550	1545	1174	1268
MgB_4	1830	1735	1273	
MgB_7	2150	2150	2509	

II. EXPERIMENTAL

A. *Electrode Preparation*

Magnesium-boron alloys were prepared using different molar ratios of boron (X_B = 0.07, 0.4, 0.73, 0.84, and 0.95) from an elemental mixture of magnesium and boron powder (both 99.99 pct pure, metal basis, purchased from Alfa Aesar). The mixing was done in an argon atmosphere glove box and transferred into a sealed jar for 24 hours jar milling to obtain a homogeneous mixture of boron and magnesium. After that, 13 mm diameter pellets were made from the homogeneous mixture using a Carver cold pressing unit at a pressure of 5000 psi for 5 minutes. The pellets were wrapped in a tantalum (Ta) foil to avoid surface oxidation, transferred into a vacuum-sealed quartz ampoule, and placed in a Fisher Scientific box furnace at 600 °C for 168 hours to get an equilibrium phase composition.

Electrodes (RE or WEs) were made using the mixture of Mg or Mg-B alloys and the eutectic mixture of CaF_2-MgF_2 (both 99.99 pct pure, metal basis, purchased from Alfa Aesar). The nominal compositions of the electrodes are summarized in Table III. These electrodes were also made into a 13 mm diameter pellet at 5000 psi for 5 minutes using a Carver cold pressing unit. Then, the electrodes were wrapped in a Ta foil and transferred into a vacuum-sealed quartz ampoule with Cu getter to avoid oxidation. Finally, the pellets were placed in a Fischer Scientific box furnace for sintering at 600 °C for 336 hours.[31]

B. *Solid-State Electrochemical Cell*

Figure 2 has shown the schematic diagram of the solid-state galvanic cell used in this study. In the previous studies, Reddy *et al.* had described the detailed experimental procedure for the determination of phase stabilities of different binary systems.[28,31–34] The solid-state emf cell was in a single compartment alumina tube. This alumina tube was placed in a vertical resistance furnace. A continuous flow of ultrahigh-purity dry argon was maintained in the compartment. A vacuum pump was continuously used to evacuate the chamber. In the argon-purged line, anhydrous calcium sulfate (dierite) and a Cu gettering furnace were utilized to eliminate residual moisture and oxygen from the argon gas, respectively. The Cu gettering furnace was maintained at 985 K. Cu getters were also used in the bottom of the main compartment to prevent any further oxidation during the experiment. The emf cell assembly (inset of Figure 1) was located in the isothermal zone of the vertical resistance furnace to maintain a uniform temperature. A type K thermocouple measured the cell temperature accurately. The emf cell assembly consists of the RE (bottom), the optical grade single-crystal CaF_2 (purchased from Sigma Aldrich, 99.99 pct metal basis), and the WEs (top). This emf assembly was sandwiched between the Pt electrodes which were connected through the Pt/Rh wire to the Keithly 2700 multimeter. This sandwiched setup was pushed from both sides by alumina disks with the spring tightened alumina pressing tube. Open circuit potential (OCP) of electrochemical cell was obtained at a constant temperature after holding for 7 to 9 hours during the heating and cooling cycle, using the Keithly 2700 multimeter. The potential variation was within ± 0.01 mV for higher boron concentrations. This small variation was considered as the stable cell potential indicating that the system had reached an equilibrium state.[31]

Table III. Nominal Composition of the Reference and Working Electrodes

Electrodes	X_B	X_{Mg}
$CaF_2 + MgF_2 + Mg$ (RE)	0	1
$CaF_2 + MgF_2 + Mg_{0.93}B_{0.07}$ (WE)	0.07	0.93
$CaF_2 + MgF_2 + Mg_{0.4}B_{0.6}$ (WE)	0.6	0.39
$CaF_2 + MgF_2 + Mg_{0.27}B_{0.73}$ (WE)	0.73	0.27
$CaF_2 + MgF_2 + Mg_{0.16}B_{0.84}$ (WE)	0.84	0.16
$CaF_2 + MgF_2 + Mg_{0.05}B_{0.95}$ (WE)	0.95	0.05

CaF_2:MgF_2 = 1:1 (molar ratio).

C. *Electrodes' (RE and WEs) Phase Equilibria and Phase Analyses*

The pure Mg and Mg-B alloys were mixed with the CaF_2-MgF_2 eutectic mixture to prepare the RE and WEs, respectively. The electrodes' phases were identified using a Philips X'pert MPD X-ray diffraction (XRD) analyzer, by varying the 2θ values from 10 to 90 deg with a step of 0.001 at 0.05 deg/s. The XRD was performed after the equilibrium measurement to validate the phase stabilities of the RE and WEs. In Figure 3, the XRD analysis confirms that no other phases are present in the RE after the equilibrium. The corresponding phases (Mg, MgF_2, and CaF_2) are indicated as a line (taken from ICDD) below the RE XRD spectrum. The PDF card of the probable competing phase $CaMg_2$ is also added below the RE XRD spectrum to compare.

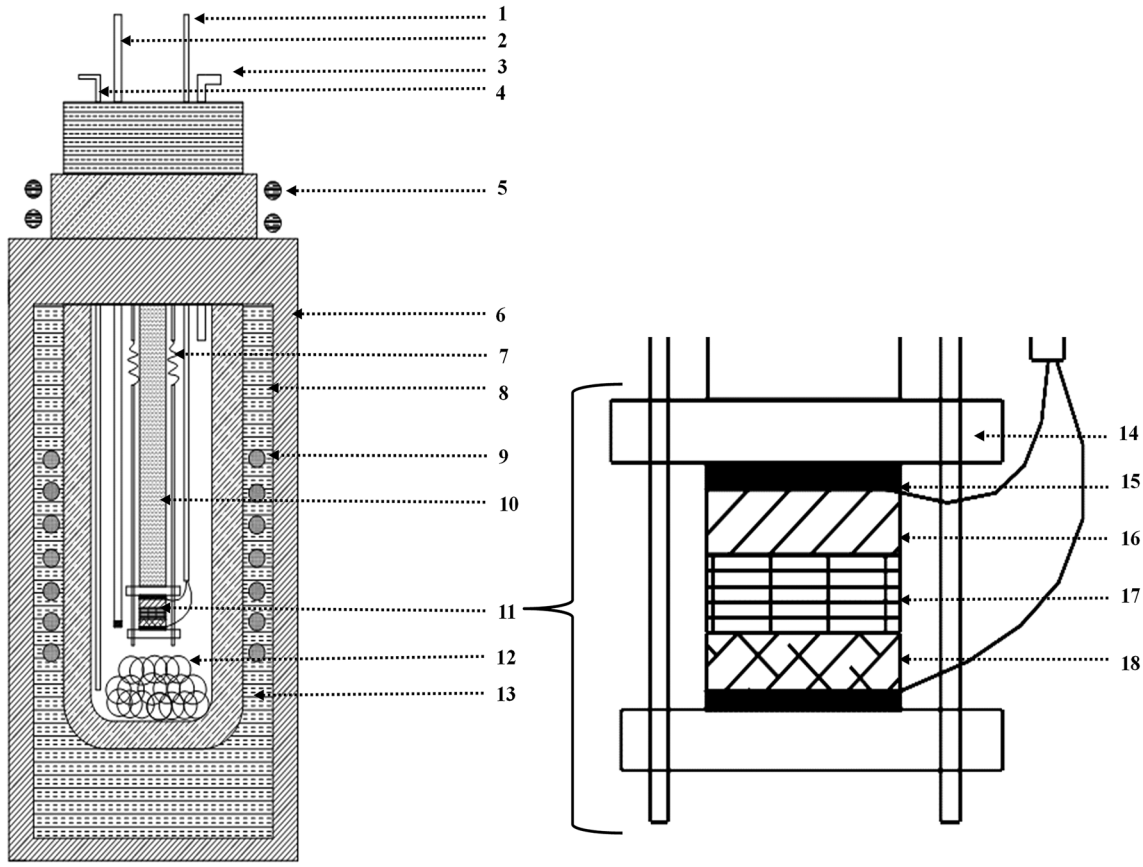

Fig. 2—Schematic cross-sectional diagram of solid-state electrochemical galvanic cell: 1—Pt/Rh wires with alumina sleeve, 2—sample thermocouple (type k), 3—gas outlet, 4—gas inlet, 5—water cooled brass flange, 6—vertical tubular furnace, 7—spring, 8—fire brick, 9—heating coil, 10—alumina pressing tube, 11—galvanic cell assembly, 12—Cu gutter, 13—alumina tube, 14—alumina support disk, 15—Pt disk, 16—working electrode, 17—CaF_2 electrolyte, and 18—reference electrode.

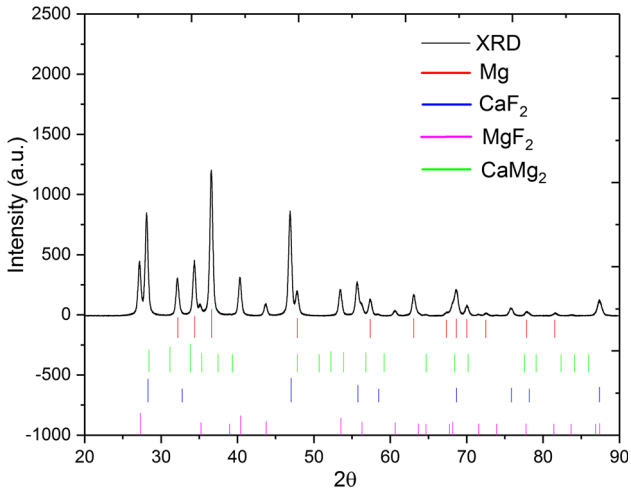

Fig. 3—X-ray diffraction of RE after emf measurements.

The XRD analysis in Figures 4(a) through (d) again confirms that other phases were not present in the WEs after the equilibrium measurements. The corresponding phases (Mg, B, MgB_2, MgB_4, MgB_7, MgF_2, and CaF_2) are shown as a line (taken from ICDD) below the WEs XRD spectrum.

In addition, a detail thermodynamic phase equilibria study was also done using Fact Sage 7 (Tables IV and V) thermodynamic software.[35] In Table IV, all the competing phases are tabulated for the different nominal composition of the electrodes with their respective activities at 600 °C. As mentioned earlier, equimolar CaF_2 and MgF_2 were added in all the electrodes. As seen from Table IV, for any particular WE, the activities of any individual phase have the value of one ($a_i = 1$), which represents the stability of that particular phase at 600 °C. In contrast, any phases contributing an activity value less than one ($a_i < 1$) represents the less-stable phase at that temperature. For example, a particular alloying composition ($Mg_{0.16}B_{0.84}$) with equimolar of CaF_2 (1 mole) and MgF_2, the phase activities [CaF_2, MgF_2, MgB_4, and $Mg(B_6)_2$] are one, which confirms that the four-phase equilibrium exists at 600 °C for this particular composition. It needs to be mentioned that the $Mg(B_6)_2$ phase is used alternatively for MgB_7 in FactSage 7 (FactPS database). In addition, one of the leading competing phases, *i.e.*, $CaMg_2$ has the activities of less than one in all the electrodes system, which confirms that the formation of $CaMg_2$ phase is thermodynamically not stable at 600 °C. In addition to this, the spontaneities of all the competing phases at the desired working temperature are summarized in Table V

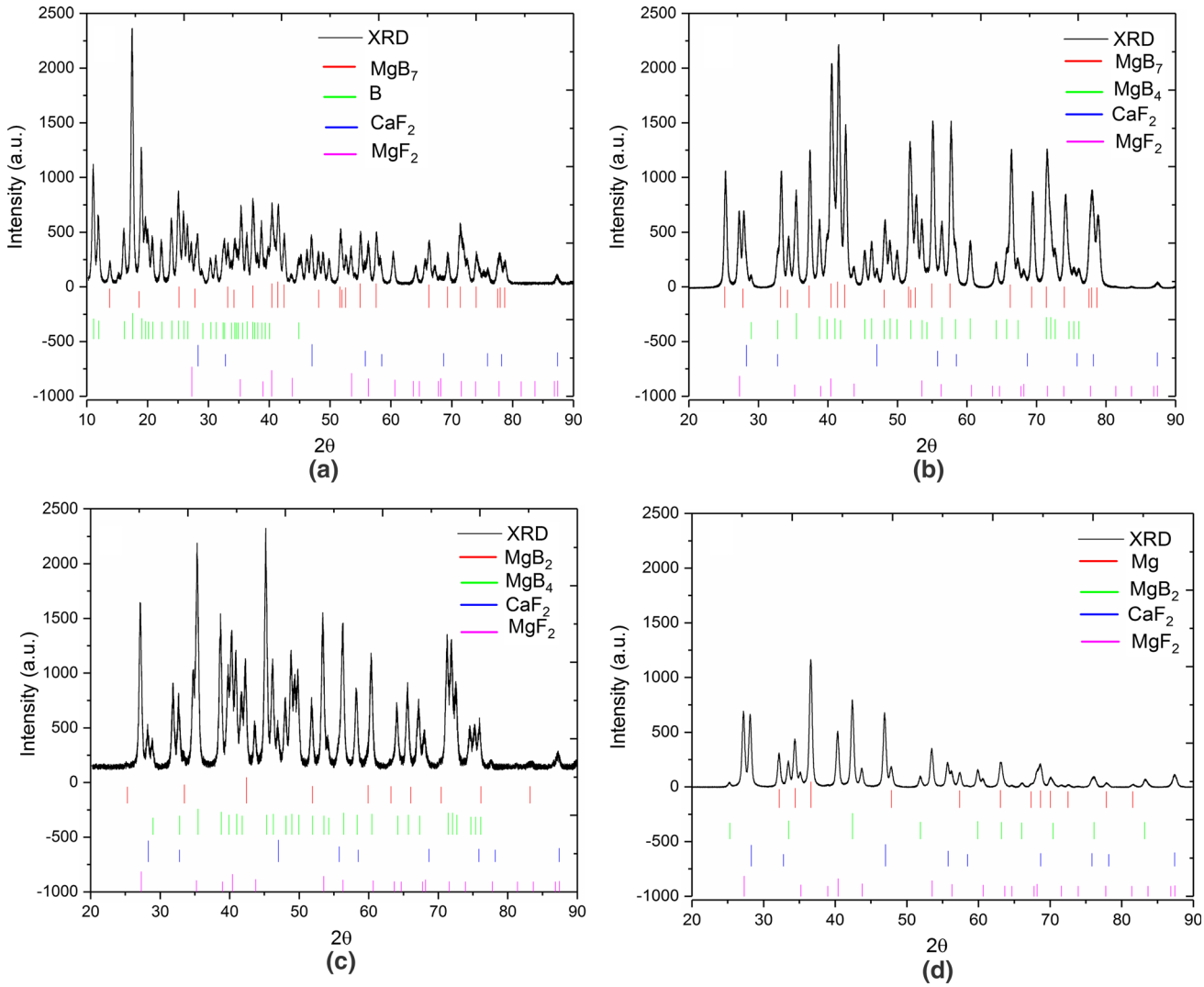

Fig. 4—X-ray diffraction of WEs after emf measurements. (*a*) B-MgB_7-MgF_2-CaF_2, (*b*) MgB_7-MgB_4-MgF_2-CaF_2, (*c*) MgB_4-MgB_2-MgF_2-CaF_2, (*d*) Mg-MgB_2-MgF_2-CaF_2.

Table IV. Thermodynamic Phase Stabilities of RE and WEs Using FactPS Database

	Activities					
Phases	Mg (RE)	$Mg_{0.93}B_{0.07}$ (WE)	$Mg_{0.4}B_{0.6}$ (WE)	$Mg_{0.27}B_{0.73}$ (WE)	$Mg_{0.16}B_{0.84}$ (WE)	$Mg_{0.05}B_{0.95}$ (WE)
MgF_2_Sellaite_(TiO_2_r(s)	1	1	1	1	1	1
CaF_2_Fluorite_(*Fm3m*)(s)	1	1	1	1	1	1
Mg_solid(s)	1	1	1	8.68×10^{-08}	5.79×10^{-09}	8.49×10^{-19}
MgB_2_hP3-P_6/mmm(s)		1	1	1	2.58×10^{-01}	1.64×10^{-09}
CaF_2_Solid-beta(s2)	5.75×10^{-01}	5.75×10^{-01}	5.75×10^{-01}	5.75×10^{-01}	5.75×10^{-01}	5.75×10^{-01}
B_Solid,_Beta-Rhomboh(s)		2.26×10^{-05}	2.26×10^{-05}	7.70×10^{-02}	1.51×10^{-01}	1
Mg_2Ca_Laves_C-14(s)	3.22×10^{-07}	3.22×10^{-07}	3.22×10^{-07}	2.11×10^{-28}	6.27×10^{-32}	1.97×10^{-61}
MgB_4_oP20-Pnam(s)		8.68×10^{-08}	8.68×10^{-08}	1	1	2.78×10^{-07}
Ca_Solid_Alpha(s)	9.43×10^{-10}	9.43×10^{-10}	9.43×10^{-10}	8.19×10^{-17}	5.46×10^{-18}	8.01×10^{-28}
Ca_Solid_Beta(s2)	9.14×10^{-10}	9.14×10^{-10}	9.14×10^{-10}	7.93×10^{-17}	5.29×10^{-18}	7.76×10^{-28}
$Mg(B_6)_2$_solid(s)		2.19×10^{-38}	2.19×10^{-38}	4.45×10^{-03}	1	1

CaF_2:MgF_2 = 1:1 (molar ratio).

Table V. The Probable Reactions of the Competing Phases and Their Spontaneities in the Electrodes Using Factsage Reaction Module

Probable Reactions for the Formation of Competing Phase	ΔG (600 °C)
$0.4\ Mg + CaF_2 + MgF_2 + 0.6B = MgF_2 + 0.1\ Mg + CaF_2 + 0.3MgB_2$	− 30,943.8
$0.27\ Mg + CaF_2 + MgF_2 + 0.73B = MgF_2 + 0.095MgB_4 + CaF_2 + 0.175\ MgB_2$	− 30,231.8
$0.16\ Mg + CaF_2 + MgF_2 + 0.84\ B = 0.2\ B + MgF_2 + 0.16\ MgB_4 + CaF_2$	− 20,515.8
$0.05\ Mg + CaF_2 + MgF_2 + 0.95B = 0.35B + MgF_2 + 0.05MgB_{12} + CaF_2$	− 9137.6
$0.27\ Mg + CaF_2 + MgF_2 + 0.73B = MgF_2 + 0.1825MgB_4 + 0.04375Mg_2Ca + 0.95Ca + F_2$	1,052,571
$0.4\ Mg + CaF_2 + MgF_2 + 0.6B = MgF_2 + 0.15MgB_4 + 0.125Mg_2Ca + 0.875\ Ca + F_2$	1,054,568
$0.4\ Mg + CaF_2 + MgF_2 + 0.6B + 1.7\ MgB_2 = MgF_2 + MgB_4 + 0.55Mg_2Ca + 0.45Ca + F_2$	1,109,574
$0.27\ Mg + CaF_2 + MgF_2 + 0.73B + - 1.635MgB_2 = MgF_2 + MgB_4 + 0.4525Mg_2Ca + 0.5475Ca + F_2$	1,105,474
$0.27\ Mg + CaF_2 + MgF_2 + 0.73B = MgF_2 + 9.50E{-}02MgB_4 + 0.001Mg_2Ca + Ca + 0.175MgB_2 + F_2$	1,046,759
$0.27\ Mg + CaF_2 + MgF_2 + 0.73B = MgF_2 + 9.50E{-}02MgB_4 + Ca + 0.175MgB_2 + F2$	1,046,908
$0.27Mg + CaF_2 + MgF_2 + 0.73B = 0.2B + MgF_2 + 0.1325MgB_4 + 0.06875Mg_2Ca + 6.88E{-}02F_2$	55,227.4
$0.16\ Mg + CaF_2 + MgF_2 + 0.84B = 0.2B + MgF_2 + 0.16MgB_4 + Ca + F_2$	1,056,625
$0.05\ Mg + CaF_2 + MgF_2 + 0.95B = 0.35\ B + MgF_2 + 0.05MgB_{12} + F_2 + Ca$	1,068,003
$Mg + 0.5CaF_2 + 0MgF_2 = 0.5CaMg_2 + 0.5F_2$	525,214.8
$Mg + 0.5CaF_2 = 0.5CaMg_2 + 0.5F_2$	525,214.8
$MgF_2 + 0.5CaF_2 = 0.5\ CaMg_2 + 1.5F_2$	1,497,427

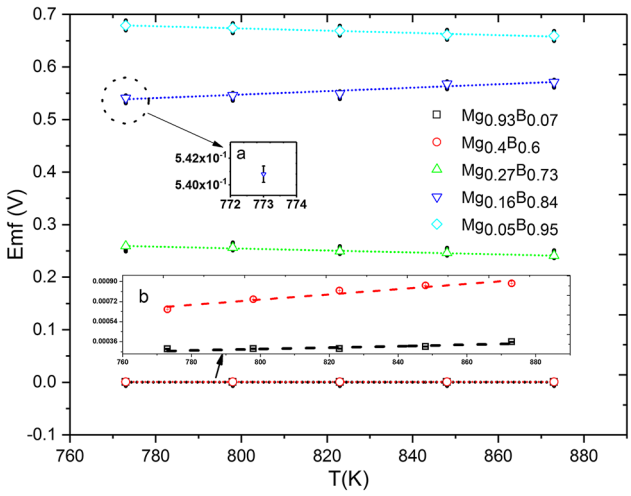

Fig. 5—Electromotive force as a function of temperature upon heating a CaF_2-based electrochemical cell with Mg-B alloy (inset figure shows (*a*) error bar at 773 K and $X_B = 0.84$, (*b*) magnifying emf *vs* T figure for $X_B = 0.07$ and 0.6).

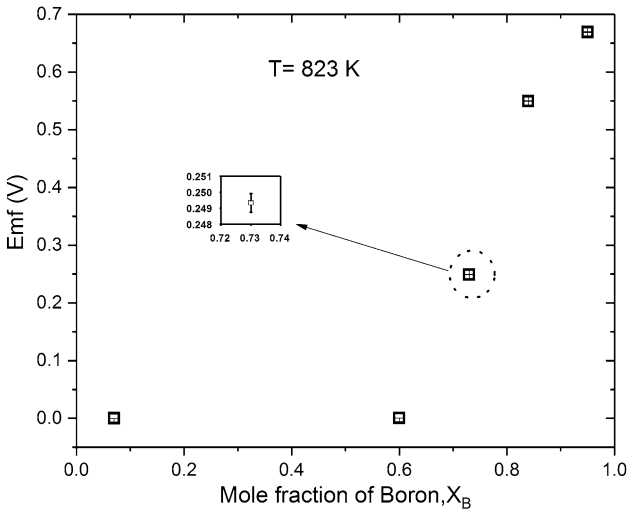

Fig. 6—Electromotive force as a function of X_B upon heating at 823 K in a CaF_2-based electrochemical cell with Mg-B alloy (inset image shows the error bar for $X_B = 0.73$).

Table VI. Measured Emf Values with the Variation of the Temperature and Composition

	Emf (mV)				
	X_B				
T (K)	0.07	0.6	0.73	0.84	0.95
773	$0.2950 \pm 9.50\times10^{-04}$	$0.651 \pm 1\times10^{-03}$	259 ± 0.15	541 ± 0.76	680 ± 0.26
798	$0.2960 \pm 6.15\times10^{-04}$	$0.741 \pm 1\times10^{-03}$	256 ± 1.00	546 ± 0.58	674 ± 0.30
823	$0.2977 \pm 2.08\times10^{-04}$	$0.821 \pm 1\times10^{-03}$	249 ± 0.58	550 ± 0.76	669 ± 0.56
848	$0.3163 \pm 1.53\times10^{-04}$	$0.865 \pm 1\times10^{-03}$	246 ± 0.57	568 ± 0.57	661 ± 0.57
873	$0.3584 \pm 2.00\times10^{-04}$	$0.884 \pm 1\times10^{-03}$	241 ± 0.81	571 ± 0.56	659 ± 0.55

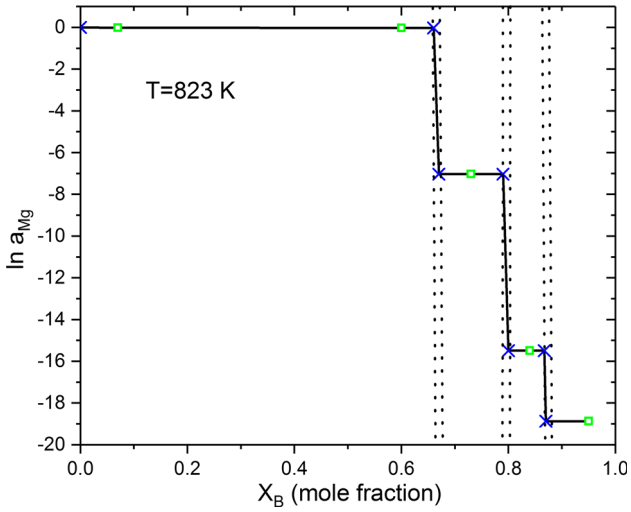

Fig. 7—Variations of activity of Mg as a function of mole fraction of B at 823 K (✕ estimated from experimental data ▢).

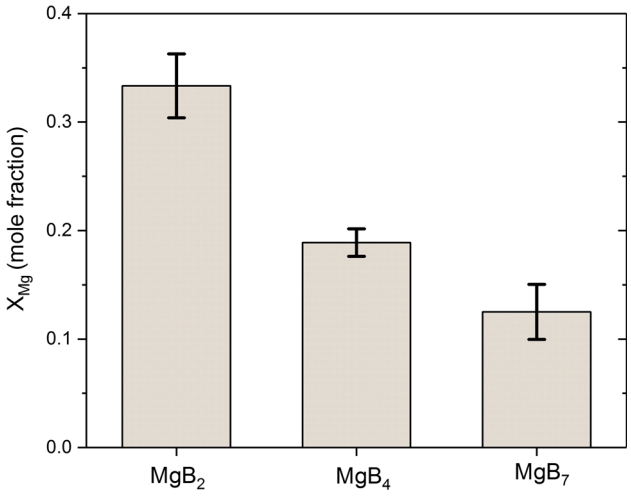

Fig. 8—Variations of Mg in different alloys of Mg-B system shown with the error bar.

using reaction module of Factsage 7. The main competing phases, such as $CaMg_2$ and Ca, are thermodynamically not possible since the Gibbs energies for those reactions are positive. This finding again confirms that the formation of these competing phases is not possible within this temperature range. These findings agree with the XRD analysis of the WEs after emf measurements. This also confirms that no other phases, such as $CaMg_2$, were formed during the emf measurements. Moreover, it has already been discussed in the previous section that the recent literature confirmed that MgB_7 is a more stable phase than MgB_{12} for a higher boride system. Therefore, MgB_{7-} was considered in this study to obtain the equilibrium measurements for higher boride system.

D. *Experimental Errors*

Errors in experimental measurements could arise from the high vapor pressure of Mg, which eventually decreases the desired Mg concentration in electrodes. For a low concentration of Mg, the measured emf value varies from 240 to 680 mV for different compositions and temperatures. The measured emf values show up to 0.15 pct error that comes from the experimental setup and the instrumental measurement technique, which is less significant compared to the emf values that are large enough. Besides, for a high concentration of Mg, the measured emf values vary from 0.296 to 0.886 mV for different temperatures and compositions. The measured emf values show up to 0.3 pct error, which is within the acceptable limit. Since the emf values are small enough in high Mg concentration, the percent error has relatively greater significant effect than that observed with low Mg concentration. This uncertainty resulted from the highly volatile nature of Mg.

III. RESULTS AND DISCUSSION

The stable open-circuit potential (emf) of the electrochemical cell represented in Eq. [1] for Mg-B alloys is shown in Figure 5 over the temperature range of 773 K to 873 K. All the emf measurements are also presented in Table VI. As seen in Figure 5, the emf data vary linearly with the temperature. No change in slope indicates the phase stabilities of these alloys over the selected temperature and compositional ranges. For the magnesium-rich solution ($X_{Mg} \geq 0.40$), the measured emf values were very small. The measured emf values *vs* T for $X_{Mg} = 0.93$ and $X_{Mg} = 0.40$ are almost invariant. In this region, $Mg + MgB_2$ are present. Pure Mg is the reason for obtaining a very lower emf value, which approaches zero with the increasing Mg concentration. This behavior agrees with the previously observed Ca-Bi, Ca-Mg, and Sr-Bi systems by Kim *et al.*[24,27] The emf values increased to ~ 0.25 V in the $MgB_2 + MgB_4$ two-phase region, and increase further in the $MgB_4 + MgB_7$ and $B + MgB_7$ two-phase regions by ~ 0.3 and ~ 0.15 V, respectively. The emf is also shown as a function of mole fraction of boron in Figure 5. As seen in Figure 5, the emf values did not change significantly in the $Mg + MgB_2$ binary region. It changed considerably after the composition crossed the MgB_2 stoichiometric line. An increasing trend of emf change was observed with the increasing mole fraction of boron (Figure 6).

In Figure 7, the natural logarithm of activity of Mg, $\ln a_{Mg}$, is presented, where the Nernst equation was used to calculate the activity of Mg at 823 K:

$$\ln a_{Mg} = -\frac{2 \times 96500 \times E_{cell}}{R \times 823} \quad [9]$$

As seen from Figure 7, the activity of Mg decreases with the increasing mole fraction of boron. The activity does not change in the two-phase regions. Using this principle, we estimated the activities of Mg in the

Table VII. Comparison of Compositional Variations of MgB_2, MgB_4, and MgB_7 by EDS Analysis with the Literature Data

MgB_2		MgB_4		MgB_7	
X_{Mg}	X_B	X_{Mg}	X_B	X_{Mg}	X_B
0.33 ± 0.029	0.67 ± 0.029	0.19 ± 0.013	0.81 ± 0.013	0.1251 ± 0.025	0.8749 ± 0.025
0.325	0.675[18]			0.131 ± 0.01[2]	0.869 ± 0.02[2]
0.32 ± 0.041	0.68 ± 0.041[13]				

Table VIII. Activities of Mg in Mg-B Alloy

		ln a_{Mg}				
X_{Mg}	X_B	773 K	798 K	823 K	848 K	873 K
0.93	0.07	− 8.28*	− 8.49*	− 8.68*	− 8.86*	− 9.05*
0.4	0.6	− 0.02	− 0.022	− 0.023	− 0.024	− 0.024
0.27	0.73	− 7.78	− 7.45	− 7.02	− 6.73	− 6.4
0.16	0.84	− 16.24	− 15.88	− 15.48	− 15.54	− 15.181
0.05	0.95	− 20.38	− 19.60	− 18.86	− 18.09	− 17.52

[*× 10^{-3}].

Table IX. Activity Coefficients of Mg in Mg-B Alloy

		γ_{Mg}				
X_{Mg}	X_B	773 K	798 K	823 K	848 K	873 K
0.93	0.07	1.06	1.07	1.07	1.07	1.07
0.4	0.6	2.45	2.44	2.44	2.44	2.44
0.27	0.73	1.55*	2.16*	3.3*	4.4*	6.1*
0.16	0.84	5.51†	7.92†	11.8†	11.1†	16†
0.05	0.95	2.8‡	6.13‡	12.8‡	27.8‡	4.92‡

[*× 10^{-3}, †× 10^{-7} and ‡× 10^{-8}].

two-phase boundaries to obtain the activity of Mg close to the MgB_2, MgB_4, and MgB_7 stoichiometric composition. The compositions of the prepared MgB_2, MgB_4 and MgB_7 are varied due to the experimental uncertainties, characterized by energy dispersive X-ray spectroscopy (EDS). In Figure 8, the variation of Mg mole fraction is shown with the error bar. In Table VII, the EDS analyses of the phases are presented and compared to those in the literature. All the activity data (ln a_{Mg}) for 773 K to 873 K are reported in Table VIII. Activity coefficients are also calculated for Mg and summarized in Table IX. The integral Gibbs energies of formation (ΔG_f°) of MgB_2, MgB_4, and MgB_7 were also estimated using the tangent rule with the measured activities of the Mg. In the two-phase region, the equal chemical potential of each component or species characterizes the equilibrium. Hence, starting from the boron-rich (B + MgB_7) equilibrium, $\frac{\Delta G_f(MgB_7)}{1/8} = \frac{RT \ln a_{Mg}}{1}$ gives the ΔG_f° (MgB_7) = − 15.89 kJ/mol-atoms at 873 K. The integral Gibbs energies of formation (ΔG_f°) for all the equilibrium phases for the range from 773 K to 873 K are summarized in Table X.

Table X. Gibbs Energies of Formation for the MgB_2, MgB_4, and MgB_7 Using Tangent Rule

	ΔG_f° (kJ/mol atoms)				
Phase	773 K	798 K	823 K	848 K	873 K
MgB_2	− 16.67	− 16.48	− 16.01	− 15.82	− 15.48
MgB_4	− 20.87	− 21.07	− 21.18	− 21.91	− 22.03
MgB_7	− 16.37	− 16.25	− 16.13	− 15.94	− 15.89

IV. CONCLUSIONS

In this study, a solid-state galvanic cell over the temperature range from 773 K to 873 K was used to determine the thermodynamic properties of the magnesium-boron binary system. The emf values for different alloys of the Mg-B system (X_B = 0.07, 0.6, 0.73, 0.84, and 0.95) were measured using a solid-state CaF_2-based emf cell. The activities of Mg in Mg-B alloys were evaluated, and the activity coefficient of Mg at each alloy was also reported. The integral Gibbs energies of formation (ΔG_f°) of MgB_2, MgB_4, and MgB_7 were also estimated using tangent rule and reported for different temperatures. The integral Gibbs energies of formation (ΔG_f°) of MgB_2, MgB_4, and MgB_7 are − 15.48, − 22.03, and − 15.89 kJ/mol-atoms at 873 K, respectively.

ACKNOWLEDGMENTS

The authors gratefully acknowledge the financial support, Grant No. DMR-1310072, provided by the National Science Foundation (NSF). The authors thank Dr. M.R. Bogala and J.S. Young for proof reading the manuscript.

REFERENCES

1. J. Nagamatsu, N. Nakagawa, T. Muranaka, Y. Zenitani, and J. Akimitsu: *Nature*, 2001, vol. 410, pp. 63–64.
2. A. Pediaditakis, M. Schroeder, V. Sagawe, T. Ludwig, and H. Hillebrecht: *Inorg. Chem.*, 2010, vol. 49, pp. 10882–93.
3. W.C. Johnson: *J. Chem. Educ.*, 1934, vol. 11, p. 256.
4. Y. Markovskii, Y.D. Kondrashev, and G.V. Kaputovskaya: *Zh. Obshch. Khim.*, 1955, vol. 25, pp. 433–44.
5. R. Naslain, A. Guette, and P. Hagenmuller: *J. Less Common Met.*, 1976, vol. 47, pp. 1–16.
6. K.E. Spear: *Boron and Refractory Borides*, V.I. Matkovich, ed., Springer, Berlin, 1977, pp. 439–456.
7. T.B. Massalski, H. Okamoto, P.R. Subramanian, L. Kacprzak, and W.W. Scott: *Binary Alloy Phase Diagrams*, American Society for Metals, Metals Park, 1986.
8. Z.K. Liu, Y. Zhong, D.G. Schlom, X.X. Xi, and Q. Li: *Calphad*, 2001, vol. 25, pp. 299–303.
9. S. Kim, D.S. Stone, J.I. Cho, C.Y. Jeong, C.S. Kang, and J.C. Bae: *J. Alloys Compd.*, 2009, vol. 470, pp. 85–89.
10. J.O. Andersson, T. Helander, L. Höglund, P. Shi, and B. Sundman: *Calphad*, 2002, vol. 26, pp. 273–312.
11. S.L. Chen, S. Daniel, F. Zhang, Y.A. Chang, X.Y. Yan, F. Xie, R.S. Fetzer, and W.A. Oates: *Calphad*, 2002, vol. 26, pp. 175–88.
12. S.D. Bohnenstiehl, M.A. Susner, S.A. Dregia, M.D. Sumption, J. Donovan, and E.W. Collings: *Thermochim. Acta*, 2014, vol. 576, pp. 27–35.
13. B. Birajdar, N. Peranio, and O. Eibl: *Microsc. Microanal.*, 2007, vol. 13, pp. 290–91.
14. D.G. Hinks, J.D. Jorgensen, H. Zheng, and S. Short: *Physica C*, 2002, vol. 382, pp. 166–76.
15. E.I. Kuznetsova, S.V. Sudareva, T.P. Krinitsina, Yu.V. Blinova, E.P. Romanov, Yu.N. Akshentsev, M.V. Degtyarev, M.A. Tihonovskiy, and I.F. Kislyak: *Phys. Met. Metallogr.*, 2014, vol. 115, pp. 175–85.
16. P. Bordet, M. Mezouar, M.N. Regueiro, M. Monteverde, M.D. Regueiro, N. Rogado, K.A. Regan, M.A. Hayward, T. He, S.M. Loureiro, and R.J. Cava: *Phys. Rev. B*, 2001, vol. 64, p. 172502.
17. X.H. Chen, Y.S. Wang, Y.Y. Xue, R.L. Meng, Y.Q. Wang, and C.W. Chu: *Phys. Rev. B*, 2001, vol. 65, p. 024502.
18. T.A. Prikhna, W. Gawalek, Y.M. Savchuk, T. Habisreuther, M. Wendt, N.V. Sergienko, V.E. Moshchil, P. Nagorny, C. Schmidt, J. Dellith, U. Dittrich, D. Litzkendorf, V.S. Melnikov, and V.B. Sverdun: *Supercond. Sci. Technol.*, 2007, vol. 20, p. S257.
19. P.W. Gilles: *J. Am. Chem. Soc.*, 1964, vol. 86, pp. 5702–03.
20. L.P. Cook, R. Klein, W.W. Ng, Q. Huang, R.A. Ribeiro, and P.C. Canfield: *IEEE Trans. Appl. Supercond.*, 2005, vol. 15, pp. 3227–29.
21. S. Brutti, A. Ciccioli, G. Balducci, G. Gigli, P. Manfrinetti, and A. Palenzona: *Appl. Phys. Lett.*, 2002, vol. 80, pp. 2892–94.
22. N.I. Sorokin and B.P. Sobolev: *Crystallogr. Rep.*, 2007, vol. 52, pp. 842–63.
23. J. Delcet, R.J. Heus, and J.J. Egan: *J. Electrochem. Soc.*, 1978, vol. 125, pp. 755–58.
24. H. Kim, D.A. Boysen, D.J. Bradwell, B. Chung, K. Jiang, A.A. Tomaszowska, K. Wang, W. Wei, and D.R. Sadoway: *Electrochim. Acta*, 2012, vol. 60, pp. 154–62.
25. S. Poizeau, H. Kim, J.M. Newhouse, B.L. Spatocco, and D.R. Sadoway: *Electrochim. Acta*, 2012, vol. 76, pp. 8–15.
26. J.M. Newhouse, S. Poizeau, H. Kim, B.L. Spatocco, and D.R. Sadoway: *Electrochim. Acta*, 2013, vol. 91, pp. 293–301.
27. N.D. Smith, T. Lichtenstein, J. Gesualdi, K. Kumar, and H. Kim: *Electrochim. Acta*, 2017, vol. 225, pp. 584–91.
28. P. George, S.C. Parida, and R.G. Reddy: *Metall. Mater. Trans. B*, 2007, vol. 38B, pp. 85–91.
29. S.C. Hu and L.C.D. Jonghe: *Ceram. Int.*, 1983, vol. 9, pp. 123–26.
30. P. Villars, K. Cenzual, and R. Gladyshevskii: *Handbook*, Walter de Gruyter GmbH & Co KG, Berlin, 2015.
31. M.A. Imam and R.G. Reddy: *Applications of Process Engineering Principles in Materials Processing, Energy and Environmental Technologies*, Springer, Cham, 2017, pp. 457–64.
32. S.C. Parida and R.G. Reddy: *J. Chem. Thermodyn.*, 2007, vol. 39, pp. 888–92.
33. R.G. Reddy, A.M. Yahya, and L. Brewer: *J. Alloys Compd.*, 2001, vol. 321, pp. 223–27.
34. S.G. Kumar, R.G. Reddy, and L. Brewer: *J. Phase Equilibr.*, 1994, vol. 15, pp. 279–84.
35. C.W. Bale, P. Chartrand, S.A. Degterov, G. Eriksson, K. Hack, R. Ben Mahfoud, J. Melançon, A.D. Pelton, and S. Petersen: *Calphad*, 2002, vol. 26, pp. 189–228.